


 Cite this: *RSC Adv.*, 2020, 10, 38033

Photo-induced self-catalysis of nano-Bi₂MoO₆ for solar energy harvesting and charge storage†

 Jiangju Si,^{ab} Changmeng Guo,^a Haojie Liu,^a Weiwei Li,^{ab} Xiaowei Guo,^{ab} Peidong Bai,^a Yanghong Liu,^a Gairong Chen^{*ab} and Ningbo Sun^{*ab}

Efficient, sustainable, and integrated energy systems require the development of novel multifunctional materials to simultaneously achieve solar energy harvesting and charge storage. Bi-based oxysalt aurivillius phase materials are potential candidates due to their typical photovoltaic effect and their pseudo-capacitance charge storage behavior. Herein, we synthesized nano-Bi₂MoO₆ as a material for both solar energy harvesting and charge storage due to its suitable band gap for absorption of visible light and its well-defined faradaic redox reaction from Bi metal to Bi³⁺. The irradiation of visible light significantly affected the electrochemical processes and the dynamics of the Bi₂MoO₆ electrode. The photo-induced self-catalytic redox mechanism was carefully explored by adding sacrificial agents in photocatalysis reaction. In accordance with the rule of energy matching, the photo-generated holes oxidized the Bi metal to Bi³⁺, and the corresponding peak current increased by 79.5% at a scanning rate of 50 mV s⁻¹. More importantly, the peak current retention rate remained higher than 92.5% during the entire 200 cycles. The photo-generated electrons facilitated a decrease of 184 mV in the overpotential of the reduction process. Furthermore, the irradiation of visible light also accelerated the ionic diffusion of the electrolyte. These investigations provide a unique perspective for the design and development of new multifunctional materials to synergistically realize solar energy harvesting and charge storage.

 Received 15th August 2020
 Accepted 8th October 2020

DOI: 10.1039/d0ra07020c

rsc.li/rsc-advances

Highly efficient and sustainable green energy conversion and storage are available solutions to the intensifying energy and environmental conservation issues.^{1–17} New integrated energy systems with simplified processes, that realize the complementarity between multiple clean energy technologies, are attracting increasing amounts of attention.^{1,4–6,9,12–14,17} Among the numerous energy conversion and storage technologies available, solar energy is one of the most promising as an abundant, low-cost, eco-friendly, and renewable energy source. Electrochemical rechargeable devices can achieve highly efficient energy conversion and storage. Therefore, it is necessary to develop an integrated system that synchronously achieves solar energy harvesting and charge storage within one device.^{1,11,18} Some photo-rechargeable electrochemical energy storage devices, such as photo-rechargeable batteries^{7,8,12,13,16,19–22} and photo-rechargeable capacitors,^{2–6,9–11,14,15,18,23–27} have been emerged. These new devices usually contain an independent solar energy harvesting unit (such as photovoltaic solar cells that include a dye-sensitized

solar cell,⁴ organometal halide perovskite cells,²³ polymer solar cell,⁹ and Si solar cells¹³), as well as separate rechargeable energy storage units (such as lithium-ion batteries,^{5,7,12,13,21} lithium oxygen batteries,²² zinc-ion batteries⁸ and flow batteries,¹⁹ supercapacitors,^{6,14,23} and hybrid capacitors²⁵), which are expensive and lead to the energy-level mismatch and ohmic transport losses at the interface between the two units.^{3,17} Thus, it is highly desirable to explore new materials that are capable of harvesting and storing energy simultaneously.^{8,25} Bi-based oxysalt aurivillius phase materials are the potential candidates due to their typical photovoltaic effect²⁸ and electrochemical energy storage behavior.^{29–40} However, there are few reports on the integrated photo-rechargeable devices that use Bi-based oxysalt,⁴¹ and the synergy mechanism between the photovoltaic effect and the electrochemical process has not yet been revealed. Here, we selected nano-Bi₂MoO₆ as the material for both solar energy harvesting and charge storage because it has a suitable band gap for the absorption in visible light,²⁸ a layered structure that favors a high electron transfer rate, and a well-defined faradaic redox from Bi metal to Bi(III).³⁶ The irradiation of visible light significantly influenced the electrochemical processes and the dynamics of the Bi₂MoO₆ electrode, and the photo-induced self-catalytic redox mechanism was carefully explored.

Nano Bi₂MoO₆ was prepared by a simple hydrothermal reaction, and the specific method was shown in the ESI.† The X-

^aSchool of Chemistry and Materials Engineering, Xinxiang University, Xinxiang, Henan 453003, China. E-mail: sunningbo682@163.com

^bHenan Photoelectrocatalytic Material and Micro-Nano Application Technology Academician Workstation, Xinxiang, Henan 453003, China

† Electronic supplementary information (ESI) available. See DOI: 10.1039/d0ra07020c



ray diffraction (XRD) test was conducted to confirm the phase of the as-prepared Bi_2MoO_6 sample. As shown in Fig. 1a, the sharp and intense diffraction peaks demonstrated that the as-prepared Bi_2MoO_6 powder had high crystallinity, and the characteristic diffraction peaks at 10.9° , 23.6° , 28.4° , 32.6° , 33.3° , 36.0° , 39.8° , 47.2° , 55.7° , 56.3° , 58.6° , and 76.2° were well indexed to (020), (111), (131), (200), (002), (151), (062), (331), (133), (262), and (400) planes of the pure orthorhombic phase of the aurivillius Bi_2MoO_6 (JCPDS card no. 21-0102), respectively.³⁵ The morphology of the Bi_2MoO_6 was investigated by scanning electronic microscopy (SEM), transmission electron microscopy (TEM) and scanning transmission electron microscopy (STEM) (Fig. 1b–h). The SEM and TEM images of the Bi_2MoO_6 showed a mixed morphology consisting of nanorods with diameters in 50–100 nm and nanosheets of 20–30 nm thickness; the elements of Bi, Mo, and O had a uniform distribution on Bi_2MoO_6 's surface by STEM coupled with energy dispersive X-ray spectroscopy (EDX) (Fig. 1d–g). Further, the lattice interplanar spacing of 0.24 nm in the high-resolution (HR)-TEM image corresponded to the (022) crystal plane of the orthorhombic Bi_2MoO_6 (Fig. 1h).³⁶ The nanostructures of the aurivillius Bi_2MoO_6 facilitate fast transportation of electrons and ions during the electrochemical and photo reactions. In addition, Fig. 1i showed the photo absorption behavior of the nano- Bi_2MoO_6 , its visible-light response could extend to 600 nm, and the band gap was 2.6 eV, thus confirming that the as-prepared nano- Bi_2MoO_6 was able to harvest the solar energy.

The electrochemical processes of the Bi_2MoO_6 electrodes were measured using a standard three-electrode system, which contained the working electrode of Bi_2MoO_6 , the platinum counter electrode, and the Hg/HgO reference electrode in a 1 M KOH electrolyte at room temperature and atmospheric pressure. The experimental measurements of the irradiation of

visible light were carried out in a 100 ml quartz electrochemical cell. A 300 W xenon arc lamp was utilized as a visible-light source, and the light intensity is 8 mW cm^{-2} . In the dark, the cyclic voltammetry (CV) curves of the Bi_2MoO_6 electrodes exhibited well-defined faradaic redox peaks at -0.35 V , -0.50 V , and -0.75 V , corresponding to the conversion of the Bi metal to Bi(III) being mediated by OH^- from the electrolyte, which clearly indicated the typical pseudo-capacitance charge storage behavior of the Bi_2MoO_6 electrode (Fig. S1†).^{31,42} Moreover, the cathodic and anodic peak currents depended linearly on the square roots of the scan rates (Fig. S2†), revealing that the diffusion of the electrolyte was a rate-controlling step during the pseudo-capacitance charge storage process of the Bi_2MoO_6 electrodes.

Under illumination of visible light, the Bi_2MoO_6 electrode showed similar pseudo-capacitance charge storage behavior to that exhibited in the dark from the CV results (Fig. S3†), but the intensity and position of anodic and cathodic peaks showed significant changes (Fig. 2a–f). Specifically, the anodic peak at -0.35 V (P_{a2}) became much sharper and its intensity increased significantly. Correspondingly, the charging platform at -0.46 V appeared much more obvious from galvanostatic charge–discharge (GCD) result (Fig. 2h). These results clearly manifested that the irradiation of visible light improved the reversibility of the oxidation reaction from Bi^0 to Bi^{3+} and enhanced the peak current of P_{a2} dramatically.⁴¹ Furthermore, we quantitatively compared the peak current of P_{a2} at different scan rates, and found that the maximum gain reached 79.5% at the scanning rate of 50 mV s^{-1} under the irradiation of visible light (Fig. 2g). In addition, the anodic peak at -0.5 V (P_{a1}) shifted negatively, demonstrating that the oxidation from metal bismuth located near the electrode–electrolyte interface to Bi^{3+}

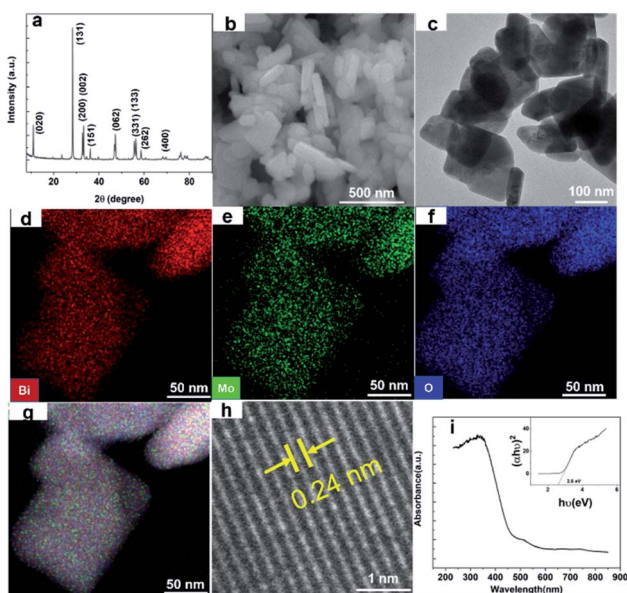


Fig. 1 (a) XRD pattern, (b) FESEM images, (c) TEM graphics, (d–g) STEM images, (h) high-resolution TEM graphic, and (i) optical absorption spectrum of the as-synthesized Bi_2MoO_6 .

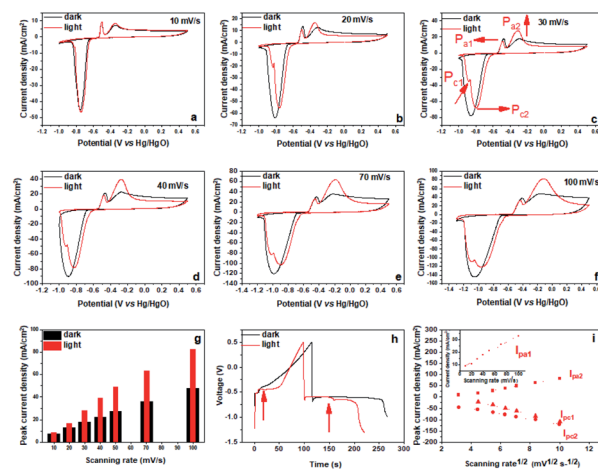


Fig. 2 (a–f) The CV curves of the Bi_2MoO_6 electrode and (g) the P_{a2} current density at different scan rates in the dark and under the irradiation of visible light; (h) the GCD profiles at 1 A g^{-1} of the Bi_2MoO_6 electrode in the dark and under the irradiation of visible light with a light intensity of 8 mW cm^{-2} ; (i) the relationship between the peak currents of the anodic and cathodic peaks and the sweep rate of the Bi_2MoO_6 electrode (the currents of the anode and cathode are abbreviated as $I_{P_{a1}}$, $I_{P_{a2}}$, $I_{P_{c1}}$ and $I_{P_{c2}}$, respectively).



occurred more easily under the irradiation of visible light.⁴³ For the reduction process, the cathodic peak at -0.74 V (P_c) had a positive shift, demonstrating that the reduction of Bi^{3+} had a smaller overpotential. Meanwhile, P_c split into a shoulder peak (P_{c1}) and a main peak (P_{c2}), also, P_{c1} became increasingly strong as the sweep rate increased. P_{c2} is attributed to the reduction of Bi^{3+} the dissolved species Bi^{3+} to Bi^0 , and the shoulder peak P_{c1} may correspond to water splitting to produce hydrogen. Simultaneously, two charging platforms arose during the discharging (Fig. 2h). These results highlighted that the irradiation of visible light had a great influence on the electrochemical behavior of the Bi_2MoO_6 electrode, and that it can improve the reversibility, decrease the overpotential and increase the peak current during the anodic and cathodic processes. Furthermore, the irradiation of visible light also affected the dynamics of the processes at the Bi_2MoO_6 electrode (Fig. 2i). As that in the dark, the transformation between Bi^0 and Bi^{3+} is still a diffusion of the electrolyte dominant process under illumination, because $I_{P_{a2}}$ and $I_{P_{c2}}$ depend linearly on the square roots of the scan rates. However, the oxidation of metal bismuth switched to a capacitive process, because $I_{P_{a1}}$ was linearly dependent on the scan rates. This result illustrated the irradiation of visible light also accelerated the mobility of ions, which enabled the diffusion of the electrolyte opposed to the rate-controlling step. Further, the electrochemical impedance spectroscopy (EIS) of the Bi_2MoO_6 electrode is performed in the dark and under the irradiation of visible light, and the results are shown in Fig. S5.† Compared with the quasi-semicircle plot in the dark condition, the Bi_2MoO_6 electrode shows a sharper plot in the low frequency region under the irradiation of visible light, verifying that the irradiation of visible light accelerated the ionic diffusion of the electrolyte again.

The above results demonstrated that the irradiation of visible light influenced the electrochemical processes and dynamics of the Bi_2MoO_6 electrode remarkably, but this influence mechanism has rarely been reported because of the complexity of the photo processes. As a typical n-type semiconductor, Bi_2MoO_6 can generate excitons, and electron-hole pairs after absorbing incident photons. Then the holes and electrons, separating in the electric field, play important roles as oxidants and reducing agents in the following process, respectively. The same photo process of the Bi_2MoO_6 also occurs in the photocatalysis reactions, and the catalytic mechanism of photo-generated carriers has been studied in depth by adding appropriate sacrificial agents.^{28,44}

Inspired by the sacrificial agents in photocatalysis, we added triethanolamine (TEA) to the electrolyte as the hole sacrificial agent to explore the influence mechanism of the photo-generated holes and electrons on the electrochemical behavior of Bi_2MoO_6 electrode. Under the irradiation of visible light, the photo-generated holes on the Bi_2MoO_6 electrode were exhausted by the TEA, avoiding the recombination of photo-generated electrons at the same time. The valence band (VB) edge of Bi_2MoO_6 located at $-0.32 + 2.6$ V (vs. NHE, pH 7), which is much lower than the oxidation potential of Bi^0 , therefore, the photo-generated holes on the Bi_2MoO_6 electrode can oxidize Bi^0 . However, there is no obvious change for the anodic peak P_{a1}

when compared with the CV curves without the TEA (Fig. 3), and only the P_{a2} declined dramatically. This result clearly confirmed that the photo-generated holes, preferring to accumulate in the bulk electrode, selectively enhanced the oxidation from Bi^0 in the electrode bulk to Bi^{3+} , but the Bi-metal in the interface cannot be oxidized. Summarizing the above oxidation process, we can find that it is the holes induced by photo on the Bi_2MoO_6 electrode, catalyze the oxidation of Bi_2MoO_6 , which means that the above oxidation process is a typical photo-induced self-catalytic oxidation reaction of Bi_2MoO_6 (Fig. 4).⁴⁵ The conduction band (CB) edge of the Bi_2MoO_6 is located at -0.32 V (vs. NHE, pH 7), which is much higher than the reduction potential of Bi^{3+} , thus, the photo-generated electrons on the Bi_2MoO_6 electrode are unable to reduce the Bi^{3+} . Meanwhile, the cathodic peak of the Bi_2MoO_6 electrode had a further positive shift, signifying that the overpotential of the reduction reaction decreased continuously, and this phenomenon became much more obvious as the scan rate increased. When the scan rate increased to 100 mV s^{-1} , the decrement in the reduction overpotential reached 184 mV (Fig. 3h), verifying the photo-induced self-catalytic reduction reaction of Bi_2MoO_6 (Fig. 4). In other words, the photo-generated electrons on the electrode can transfer rapidly to an external circuit and accelerate the reduction of the Bi_2MoO_6 electrode.

The stability of the Bi_2MoO_6 electrode under the irradiation of visible light was further investigated by cycling at a scan rate of 50 mV s^{-1} , and the results were shown in Fig. 5 and S4.† For the entire 200 cycles, the peak current retention rate of P_{a2} maintained higher than 92.5%, suggesting that photo-generated holes on the Bi_2MoO_6 electrode had a good stability. For the reduction process, the potential of P_{c2} continued to shift slightly to positive direction, but the P_{c2} had an obvious decay (Fig. S4†), the possible reason was the reduction of water.

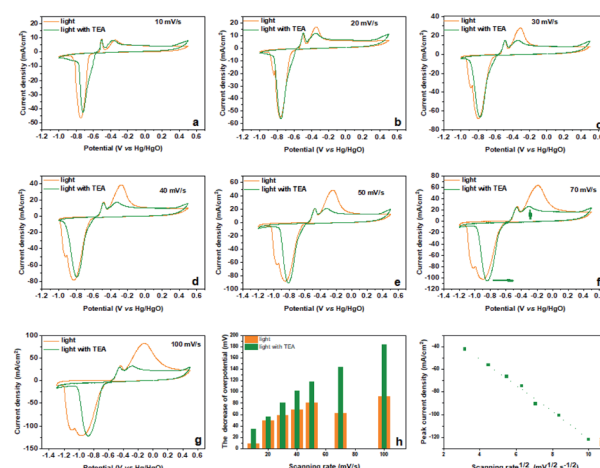
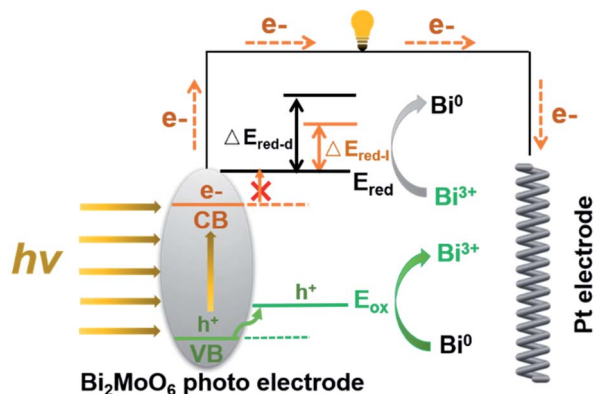


Fig. 3 (a–g) The CV curves of the Bi_2MoO_6 electrode at different scan rates and (h) the decrement in the reduction overpotential of the reduction reaction under the irradiation of visible light before and after the addition of the TEA, and the visible light intensity is 8 mW cm^{-2} ; (i) the relationship between the peak current of the cathodic peak and the sweep rate of the Bi_2MoO_6 electrode.





E_{ox} : Potential of oxidation; E_{red} : Potential of reduction
 ΔE_{red-d} : Overpotential of reduction in dark condition
 ΔE_{red-l} : Overpotential of reduction in light condition

Fig. 4 The proposed photo-induced self-catalytic redox mechanism of the Bi_2MoO_6 electrode under the irradiation of visible light.

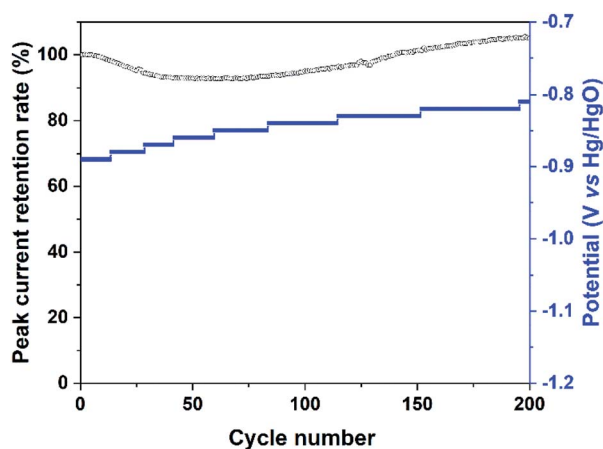


Fig. 5 The peak current retention rate of P_{a2} and the potential of P_{c2} in the CV curves of the Bi_2MoO_6 electrode cycling at a scan rate of 50 mV s^{-1} under the irradiation of visible light.

In summary, we aimed to develop novel multifunctional materials to achieve solar energy harvesting and charge storage synchronously. Nano- Bi_2MoO_6 was synthesized as a material for both solar energy harvesting and charge storage due to its suitable band gap for the absorption in visible light and its well-defined faradaic redox from Bi metal to Bi^{3+} . The irradiation of visible light had a considerable influence on the electrochemical processes and the dynamics of the Bi_2MoO_6 electrode. In accordance with the rule of energy matching, the photo-generated holes could oxidize the Bi metal to Bi^{3+} , and the photo-generated electrons could decrease the overpotential of the reduction process. Furthermore, the irradiation of visible light also accelerated the ionic diffusion of the electrolyte. This work provides a unique perspective for the development of new multifunctional materials to simultaneously achieve solar energy harvesting and electrical energy storage, and thereby

open pathways towards the efficient integrated energy systems with simplified processes.

Conflicts of interest

There are no conflicts to declare.

Acknowledgements

This work was financially supported by grants from the National Natural Science Foundation of China (No. 51901200, U1904189, 51801171), Key Scientific Research Project Plans of Higher Education Institutions in Henan Province (No. 20B430015), and the Regional Joint Fund of Basic and Applied Basic Research of Guangdong Province (No. 2019A1515110725).

References

- 1 T. Chen, L. Qiu, Z. Yang, Z. Cai, J. Ren, H. Li, H. Lin, X. Sun and H. Peng, *Angew. Chem., Int. Ed.*, 2012, **51**, 11977–11980.
- 2 Y. Jin, Z. Li, L. Qin, X. Liu, L. Mao, Y. Wang, F. Qin, Y. Liu, Y. Zhou and F. Zhang, *Adv. Mater. Interfaces*, 2017, **4**, 1700704.
- 3 E. Navarrete-Astorga, D. Solis-Cortes, J. Rodriguez-Moreno, E. A. Dalchiele, R. Schrebler, F. Martin and J. R. Ramos-Barrado, *Chem. Commun.*, 2018, **54**, 10762–10765.
- 4 T. Song and B. Sun, *ChemSusChem*, 2013, **6**, 408–410.
- 5 Y. Fu, H. Wu, S. Ye, X. Cai, X. Yu, S. Hou, H. Kafafy and D. Zou, *Energy Environ. Sci.*, 2013, **6**, 805–812.
- 6 X. Chen, H. Sun, Z. Yang, G. Guan, Z. Zhang, L. Qiu and H. Peng, *J. Mater. Chem. A*, 2014, **2**, 1897–1902.
- 7 A. Lee, M. Vörös, W. M. Dose, J. Niklas, O. Poluektov, R. D. Schaller, H. Iddir, V. A. Maroni, E. Lee, B. Ingram, L. A. Curtiss and C. S. Johnson, *Nat. Commun.*, 2019, **10**, 4946.
- 8 B. D. Boruah, A. Mathieson, B. Wen, S. Feldmann, W. M. Dose and M. De Volder, *Energy Environ. Sci.*, 2020, **13**, 2414–2421.
- 9 Z. Zhang, X. Chen, P. Chen, G. Guan, L. Qiu, H. Lin, Z. Yang, W. Bai, Y. Luo and H. Peng, *Adv. Mater.*, 2014, **26**, 466–470.
- 10 F. Zhou, Z. Ren, Y. Zhao, X. Shen, A. Wang, Y. Y. Li, C. Surya and Y. Chai, *ACS Nano*, 2016, **10**, 5900–5908.
- 11 S. Safshekan, I. Herraiz-Cardona, D. Cardenas-Morcoso, R. Ojani, M. Haro and S. Gimenez, *ACS Energy Lett.*, 2017, **2**, 469–475.
- 12 W. Guo, X. Xue, S. Wang, C. Lin and Z. L. Wang, *Nano Lett.*, 2012, **12**, 2520–2523.
- 13 H.-D. Um, K.-H. Choi, I. Hwang, S.-H. Kim, K. Seo and S.-Y. Lee, *Energy Environ. Sci.*, 2017, **10**, 931–940.
- 14 R. Liu, Y. Liu, H. Zou, T. Song and B. Sun, *Nano Res.*, 2017, **10**, 1545–1559.
- 15 H. Meng, S. Pang and G. Cui, *ChemSusChem*, 2019, **12**, 3431–3447.
- 16 A. Gurung and Q. Qiao, *Joule*, 2018, **2**, 1217–1230.
- 17 B. Luo, D. Ye and L. Wang, *Adv. Sci.*, 2017, **4**, 1700104.
- 18 A. Das, S. Deshagani, R. Kumar and M. Deepa, *ACS Appl. Mater. Interfaces*, 2018, **10**, 35932–35945.



- 19 N. F. Yan, G. R. Li and X. P. Gao, *J. Mater. Chem. A*, 2013, **1**, 7012.
- 20 P. Liu, H. X. Yang, X. P. Ai, G. R. Li and X. P. Gao, *Electrochem. Commun.*, 2012, **16**, 69–72.
- 21 A. Paoletta, C. Faure, G. Bertoni, S. Marras, A. Guerfi, A. Darwiche, P. Hovington, B. Commarieu, Z. Wang, M. Prato, M. Colombo, S. Monaco, W. Zhu, Z. Feng, A. Vijh, C. George, G. P. Demopoulos, M. Armand and K. Zaghib, *Nat. Commun.*, 2017, **8**, 14643.
- 22 H. Gong, T. Wang, H. Xue, X. Fan, B. Gao, H. Zhang, L. Shi, J. He and J. Ye, *Energy Storage Materials*, 2018, **13**, 49–56.
- 23 R. Liu, C. Liu and S. Fan, *J. Mater. Chem. A*, 2017, **5**, 23078–23084.
- 24 B. J. Trzeźniewski and W. A. Smith, *J. Mater. Chem. A*, 2016, **4**, 2919–2926.
- 25 D. B. D. Boruah, A. Mathieson, B. Wen, C. Jo, F. Deschler and M. De Volder, *Nano Lett.*, 2020, **20**(8), 5967–5974.
- 26 B. D. Boruah and A. Misra, *ACS Appl. Energy Mater.*, 2019, **2**, 278–286.
- 27 T. N. Murakami, N. Kawashima and T. Miyasaka, *Chem. Commun.*, 2005, **26**, 3346–3348.
- 28 H. Yu, L. Jiang, H. Wang, B. Huang, X. Yuan, J. Huang, J. Zhang and G. Zeng, *Small*, 2019, **15**, e1901008.
- 29 X. Hu, W. Zhang, X. Liu, Y. Mei and Y. Huang, *Chem. Soc. Rev.*, 2015, **44**, 2376–2404.
- 30 J. Wen, S. Sun, B. Zhang, N. Shi, X. Liao, G. Yin, Z. Huang, X. Chen and X. Pu, *RSC Adv.*, 2019, **9**, 4693–4699.
- 31 B. Senthilkumar, R. K. Selvan, L. Vasylechko and M. Minakshi, *Solid State Sci.*, 2014, **35**, 18–27.
- 32 Z.-Q. Liu, L.-Y. Tang, N. Li, K. Xiao, J. Wang, J.-H. Zhang, Y.-Z. Su and Y.-X. Tong, *J. Electrochem. Soc.*, 2012, **159**, D582–D586.
- 33 D. Zhu, W. Wang, J. Zhu, S. Chen and X. Liu, *J. Solid State Electrochem.*, 2016, **21**, 403–408.
- 34 F. Wu, X. Wang, W. Zheng, H. Gao, C. Hao and C. Ge, *Electrochim. Acta*, 2017, **245**, 685–695.
- 35 T. Yu, Z. Li, S. Chen, Y. Ding, W. Chen, X. Liu, Y. Huang and F. Kong, *ACS Sustainable Chem. Eng.*, 2018, **6**, 7355–7361.
- 36 K. J. Samdani, J. H. Park, D. W. Joh and K. T. Lee, *ACS Sustainable Chem. Eng.*, 2018, **6**, 16702–16712.
- 37 P. V. Shinde, N. M. Shinde, J. M. Yun, R. S. Mane and K. H. Kim, *ACS Omega*, 2019, **4**, 11093–11102.
- 38 S. S. Patil, D. P. Dubal, V. G. Deonikar, M. S. Tamboli, J. D. Ambekar, P. Gomez-Romero, S. S. Kolekar, B. B. Kale and D. R. Patil, *ACS Appl. Mater. Interfaces*, 2016, **8**, 31602–31610.
- 39 A. Martínez-de la Cruz, S. Obregón Alfaro, E. López Cuéllar and U. Ortiz Méndez, *Catal. Today*, 2007, **129**, 194–199.
- 40 J. Hu, Y. Xie, J. Zheng, Y. Lai and Z. Zhang, *Nano Res.*, 2020, **13**, 2650–2657.
- 41 M. Zargazi and M. H. Entezari, *Ultrason. Sonochem.*, 2020, **67**, 105145.
- 42 V. D. Nithya, R. Kalai Selvan, D. Kalpana, L. Vasylechko and C. Sanjeeviraja, *Electrochim. Acta*, 2013, **109**, 720–731.
- 43 V. Vivier, A. Régis, G. Sagon, J. Y. Nedelec, L. T. Yu and C. Cachet-Vivier, *Electrochim. Acta*, 2001, **46**, 907–914.
- 44 Z. Wang, H.-C. Chiu, A. Paoletta, R. Gauvin, K. Zaghib and G. P. Demopoulos, *Sustainable Energy Fuels*, 2020, **4**, 4789–4799.
- 45 S. H. DuVall and R. L. McCreery, *J. Am. Chem. Soc.*, 2000, **122**, 6759–6764.

